EurjChem
An International Open Access Journal

European **J**ournal of **Chem**istry

APH
ATLANTA PUBLISHING HOUSE

Check for updates

Mechanistic insight into propane dehydrogenation into propylene over chromium (III) oxide by cluster approach and Density Functional Theory calculations

Toyese Oyegoke [ID] 1,*, Fadimatu Nyako Dabai [ID] 1, Adamu Uzairu [ID] 2 and Baba El-Yakubu Jibril [ID] 1

1 *Chemical Engineering Department, Faculty of Engineering, Ahmadu Bello University, Zaria 234, Nigeria*
oyegoketoyese@gmail.com (O.Y.), fndabai@abu.edu.ng (F.N.D.), byjibril@gmail.com (B.Y.J.)
2 *Chemistry Department, Faculty of Physical Sciences, Ahmadu Bello University, Zaria 234, Nigeria*
adamuuzairu@gmail.com (A.U.)

* *Corresponding author at: Chemical Engineering Department, Faculty of Engineering, Ahmadu Bello University, Zaria 234, Nigeria.*
 e-mail: *toyegoke@abu.edu.ng (T. Oyegoke).*

RESEARCH ARTICLE

ABSTRACT

A preliminary study to provides insight into the kinetic and thermodynamic assessment of the reaction mechanism involved in the non-oxidative dehydrogenation (NOD) of propane to propylene over Cr_2O_3, using a density functional theory (DFT) approach, has been undertaken. The result obtained from the study presents the number of steps involved in the reaction and their thermodynamic conditions across different routes. The rate-determining step (RDS) and a feasible reaction pathway to promote propylene production were also identified. The results obtained from the study of the 6-steps reaction mechanism for dehydrogenation of propane into propylene identified the first hydrogen abstraction and hydrogen desorption to be endothermic. In contrast, other steps that include propane's adsorption, hydrogen diffusion, and the second stage of hydrogen abstraction were identified as exothermic. The study of different reaction routes presented in the energy profiles confirms the Cr-O (S1, that is, the reaction pathway that activates the propane across the Cr-O site at the alpha or the terminal carbon of the propane) pathway to be the thermodynamically feasible pathway for the production of propylene. The first hydrogen abstraction step was identified as the potential rate-determining step for defining the rate of the propane dehydrogenation process. This study also unveils that the significant participation of Cr sites in the propane dehydrogenation process and how the Cr high surface concentration would hinder the desorption of propylene and thereby promote the production of undesired products due to the stronger affinity that exists between the propylene and Cr-Cr site, which makes it more stable on the surface. These findings thereby result in Cr-site substitution suggestion to prevent deep dehydrogenation in propane conversion to propylene. This insight would aid in improving the catalyst performance.

1. Introduction

Dehydrogenation is well known to be a value addition process, especially for saturated hydrocarbons. It is a highly endothermic process that requires temperature of 500 °C and above [1,2]. Such severe reaction conditions lead to cracking of both the reactant and products and catalyst deactivation due to coke deposition. The dehydrogenation process involves converting materials like alkanes, which are of low value, to alkenes, which are known to be more reactive and valuable; an example of this is propane conversion to propylene. Propylene serves as precursors to essential products such as alcohols, aromatics, aldehydes, and polymer production [1]. It is one of the most vital building blocks in the world petrochemical industry, where it finds applications in the production of propylene oxide, isopropanol, polypropylene, and acrylonitrile [3,4].

Research has been carried out to improve the efficiency and effectiveness of propane dehydrogenation into propylene. For example, Yan *et al.* [5] employed a DFT calculation to examine gallium oxide's effectiveness in enhancing propane dehydrogenation. The study proposed a radical mechanism and identified H's abstraction from the propyl species as the rate-determining step. It was also identified that the propane dehydrogenation over $Ga_2O_3(100)$ was majorly driven by the Ga site, which was reported to actively promote the production of propylene on the gallium oxide surface.

Another DFT calculation, studied by Ming-Lei *et al.* [6], showed that with Sn on Pt catalyst, the Pt *d*-band broadened, which gave rise to a downshift in the *d*-band on the PtSn surface. The propyl and propylene bond strength to the alloyed surfaces was confirmed to be lowered, which resulted in the simultaneous decrease in the activation energy (or barrier) for propylene desorption and an increase in the activation barrier for propylene dehydrogenation.

$$H_{linear(T)} = \left[\frac{5}{2}RT\right]_{trans} + [RT]_{rot} + \left[RT\sum_i \frac{hv_i}{k_BT}\frac{e^{-\frac{hv_i}{k_BT}}}{1-e^{\frac{hv_i}{k_BT}}}\right]_{vib} \tag{1}$$

$$H_{non-linear}(T) = \left[\frac{5}{2}RT\right]_{trans} + \left[\frac{3}{2}RT\right]_{rot} + \left[RT\sum_i \frac{hv_i}{k_BT}\frac{e^{-\frac{hv_i}{k_BT}}}{1-e^{\frac{hv_i}{k_BT}}}\right]_{vib} \tag{2}$$

$$ZPE = \frac{1}{2}\sum v_{n,i} \tag{3}$$

$$s_{linear}(T) = R\left[\ln\frac{\{(2\pi m/h^2)\}^{\frac{3}{2}}(k_BT)^{\frac{5}{2}}}{P_o} + \frac{5}{2}\right]_{trans} + R\left[\ln\frac{8\pi^2 k_B T I_{r,linear}}{h^2\rho_r} + 1\right]_{rot} + \left[R\sum_i \frac{\frac{hv_i}{k_BT}}{e^{\frac{hv_i}{k_BT}}-1} - R\sum_i \ln\left(1-e^{\frac{hv_i}{k_BT}}\right)\right]_{vib} \tag{4}$$

$$s_{non-linear}(T) = R\left[\ln\frac{\{(2\pi m/h^2)\}^{\frac{3}{2}}(k_BT)^{\frac{5}{2}}}{P_o} + \frac{5}{2}\right]_{trans} + R\left[\ln\frac{8\pi^2(2\pi k_B)^{\frac{3}{2}}(T)^{\frac{3}{2}}(I_aI_bI_c)^{\frac{1}{2}}}{h^3\rho_r} + \frac{3}{2}\right]_{rot} + \left[R\sum_i \frac{\frac{hv_i}{k_BT}}{e^{\frac{hv_i}{k_BT}}-1} - R\sum_i \ln\left(1-e^{\frac{hv_i}{k_BT}}\right)\right]_{vib} \tag{5}$$

$$S_{config} = R\left[\ln\left(\frac{1-\theta}{\theta}\right) - \frac{\ln(1-\theta)}{\theta}\right] \tag{6}$$

$$S_{config} = 1.39R \tag{7}$$

These findings agree with the report of Lauri and Karoliina [7], which indicates that alloying weakens the binding of propylene and therefore prevents further dehydrogenation.

According to Ming-Lei *et al.* [6], Sn aids in increasing the catalyst selectivity for propylene production, which means Pt_3Sn bulk alloy would be an excellent potential catalyst for propane dehydrogenation. Lauri and Karoliina's [7] study also indicated that Pt-Sn alloyed catalyst's low coking and high selectivity were due to the lack of active Pt step sites.

Other related studies include Timothy [8], which shows that Pt has a poor selectivity for olefins, promotes several side reactions, and leads to the catalyst's deactivation. The study reveals that PtGa alloy has a better catalytic performance compared to SnPt; because Sn reduces the catalyst activity. Stephanie *et al.* [9] found that an increase in hydrogen pressure would decrease the coverage of deeply dehydrogenated coke precursors like ethylidyne (CCH_3) and methylidyne (CH) on the surface of Pt catalyst. It was confirmed that the rise in hydrogen coverage decreases the binding force adsorbing propylene to the Pt surface and increases the activation (or energy) barrier for the further dehydrogenation of propylene. Oyegoke *et al.* [10] indicated that Cr was highly acidic and reactive and was the active site promoting propane dehydrogenation. Other studies include Zhang *et al.* [11] work, which studied V_2O_3; Araujo-Lopez *et al.* [12] work, which studied the palladium surface; Ningning *et al.* [13] work, which studied the single vanadium atoms anchored in a graphitic carbon nitride surface; Keith *et al.* [14] work, which studied Ga-Pt supported surface; and Xie *et al.* [15] work, which studied V_2O_3 supported surface.

Most computational studies in the literature have focused mainly on Pt catalysts, with less attention being given to chromium oxide catalysts, its performance, and how it can be upgraded. This study evaluates the potential route to produce propylene across the chromium (III) oxide surface. The study provides an insight into the kinetic and thermodynamic evaluation of the reaction mechanism for the non-oxidative dehydrogenation of propane to propylene on chromium oxide using density functional theory and the cluster approach. The results obtained would allow a better understanding of the reaction and provide insight into improving the catalyst.

2. Methods

2.1. Theoretical background

In this study, the computations were carried out using the DFT calculation method in the Spartan 18 Software package and ran on an HP 15 Pavilion Notebook (Intel Core i3 Processor @ 1.8 GHz and 6 GB RAM). The catalyst, reactant, and intermediate species structures were built and minimized using the molecular mechanics (MMFF) method to remove strain energy. All molecular mechanics optimized geometries were subjected to DFT, and the B3LYP calculation method was adopted, ensuring that the structures built do not show any negative imaginary frequency on the infrared (IR) spectra results. The 6-31G* and LANL2DZ basis sets were employed because the literature confirms it to be cost-effective computationally for studies involving transition metals, such as chromium [16]. Studies indicate that a 6-31G* basis set, which is widely considered the best compromise in terms of accuracy and speed, is the most frequently used basis set available for H-Kr elements. Simultaneously, heavier atoms were modeled using the LANL2DZ basis set, which uses an effective core for all atoms larger than Ne [16,17].

The chromium (III) oxide catalyst cluster or slab (Figure 1) used in this study was adopted from Brown *et al.* [16], and it was confirmed to be similar to that used in the literature [19-21]. IR spectrum calculation was carried out with the use of Spartan 18. The calculated IR spectrum was compared with that reported in the literature to understand the cluster model's accuracy adopted for this study's chromium oxide catalyst. This comparative assessment approach was adopted from the literature [22-24] to investigate the agreement between the model and experimental values.
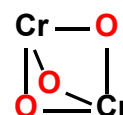

Figure 1. Molecular structure of catalyst cluster.

2.2. Thermodynamic calculation of free energy

An estimation of the thermodynamic properties of all concerned species was carried out. This calculation was done using various statistical thermodynamic models and output files collected from Spartan 18's DFT calculations. This DFT calculation provides a moment of inertia (I), total mass (m), and wavenumber (v) of the structures considered in this study, which were later used to compute the Gibbs free energy (G). The models employed were adapted from the literature [25-27] and are presented in Equations (1-7).
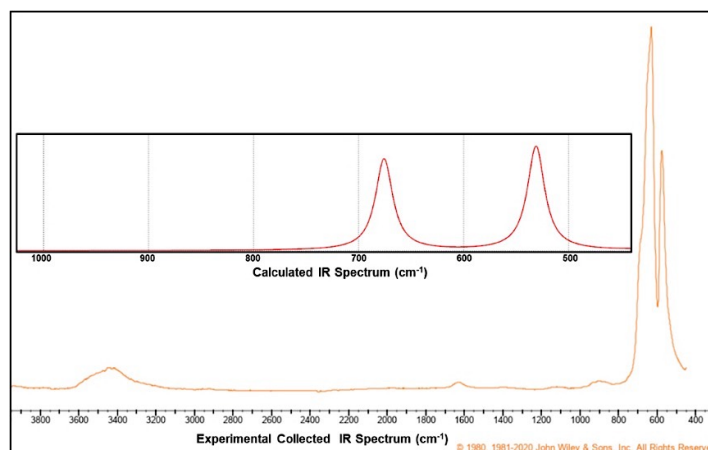
Figure 2. Chromium (III) oxide catalyst IR spectra obtained from different approaches.

Thermodynamic properties for the chemical species in this study employed the following conditions and models in the computation of Gibb free energy (G).

2.2.1. Gas-phase species

The properties of gas-phase species were computed, taking account of all contributions (that is, translational, rotational, and vibrational motion effects) to the overall thermodynamic parameters that yield the species' free energies in the reaction steps.

$$G_{gas} = H_t + H_r + H_v + E_{elect} + ZPE - T(s_t + s_r + s_v) \qquad (8)$$

2.2.2. Catalyst slab

All effects of translation and rotation were taken to be zero for the catalyst species since the catalyst is fixed, being a solid catalyst in the estimation of the catalyst-free energy.

$$G_{cat} \approx E_{elect} + ZPE + H_v - T(s_v) \qquad (9)$$

2.2.3. Surface species

The contribution of vibrational motion was thoroughly considered. Nevertheless, a half (1/2) rotational motion and two-thirds (2/3) translational contributions were considered in the estimation of the adsorbate's free energy (i.e., the surface species), with the inclusion of catalyst configuration effect on the total free energy.

$$G_{ads} = H_v + \frac{2}{3}H_t + \frac{1}{2}H_r + E_{elect} + \\ ZPE - T\left(s_v + \frac{2}{3}s_t + \frac{1}{2}s_r + s_{config}\right) \qquad (10)$$

A 2-D gas approximation [28,29] was employed in this study to treat the adsorbate with the use of hinder rotor / hindered translator models as an alternative harmonic oscillation approximation. This accounts for the loss of a degree of freedom in both translational and rotation motion contributions in an adsorbate [30,31], which has underestimated the contribution of rotation and translational motion effects in the computation of adsorbates' free energies. Where, E_{elect} = Electronic energies, G = Gibb free energies, H = Enthalpy, kB = Boltzmann constant, Po= Standard pressure, R = Gas constant, S = Entropy, T = Temperature, ZPE = Zero-point energy, r = Rotational effect contributions, t = Translational effect contributions, and v = Vibrational effect contributions.

2.3. Reaction mechanism scheme

This reaction initiates with the adsorption of propane on the catalyst surface. Next was the activation of propane across the C-H bond to give isopropyl (1-propyl and 2-propyl). This propyl further undergoes a second hydrogen abstraction to provide adsorbed propylene on the catalyst surface. The reaction ends with the desorption of both propylene and hydrogen gas from the surface of the catalyst.

The mechanism for the entire propane dehydrogenation process is presented using chemical equations, where a series of chemical equations are used to showcase the necessary elementary reaction steps involved in this study. It should be noted that the isopropyl(s) could be either 1-propyl or 2-propyl. The X denotes a catalyst site, chromium (Cr), or oxygen (O) site.
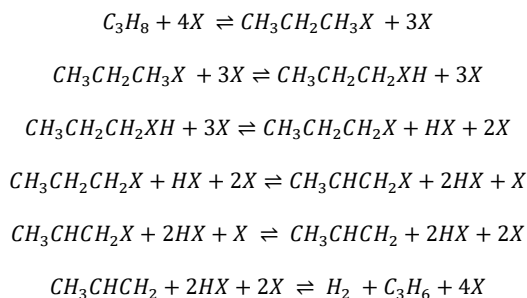
3. Results and discussions

The IR spectrum obtained for the catalyst cluster used in this study was compared with the IR spectrum collected from an experimental study obtained from Bio-Rad Laboratories, Inc. SpectraBase (Figure 2) [32]. The findings from the dehydrogenation of propane into propylene carried out over the chromium oxide catalyst evaluated for the Cr-Cr, Cr-O, O-Cr, and O-O sites, assessed using Schemes 1 and 2 as represented in Figures 3-8, are presented in this section. It was generally identified that all reaction mechanism evaluated across the different site pairs entails six elementary steps, which indicate different reaction and activation energies for propane activated across different sites or points.
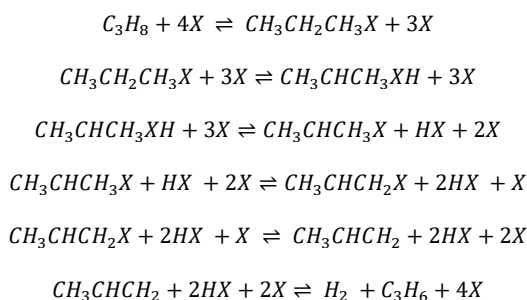
3.1. Evaluation of catalyst cluster accuracy in the modelling of Cr_2O_3

An IR spectrum experimentally collected for chromium oxide catalysts from Bio-Rad [32] and the IR spectrum for the catalyst cluster obtained from the density functional theory calculation carried in Spartan 18 modeling software are presented in Figure 2.

The study of the IR spectra in Figure 2 reveals that the experimentally determined IR spectra displayed peaks around 670 and 550 cm^{-1}, while the computationally determined IR spectra with its peaks around 675 and 545 cm^{-1} show a good agreement with the experiment. The findings indicate that the catalyst cluster used in this study to model chromium oxide fits well with the experimental results, suggesting that further deductions made from it would be reliable. It also confirms that the model adapted from Brown *et al.* [18] is satisfactory since it

$$C_3H_8 + 4X \rightleftharpoons CH_3CH_2CH_3X + 3X$$

$$CH_3CH_2CH_3X + 3X \rightleftharpoons CH_3CH_2CH_2XH + 3X$$

$$CH_3CH_2CH_2XH + 3X \rightleftharpoons CH_3CH_2CH_2X + HX + 2X$$

$$CH_3CH_2CH_2X + HX + 2X \rightleftharpoons CH_3CHCH_2X + 2HX + X$$

$$CH_3CHCH_2X + 2HX + X \rightleftharpoons CH_3CHCH_2 + 2HX + 2X$$

$$CH_3CHCH_2 + 2HX + 2X \rightleftharpoons H_2 + C_3H_6 + 4X$$

Scheme 1. The initial propane activated via the use of alpha-carbon (that is, terminal or first carbon) (**S1**).

$$C_3H_8 + 4X \rightleftharpoons CH_3CH_2CH_3X + 3X$$

$$CH_3CH_2CH_3X + 3X \rightleftharpoons CH_3CHCH_3XH + 3X$$

$$CH_3CHCH_3XH + 3X \rightleftharpoons CH_3CHCH_3X + HX + 2X$$

$$CH_3CHCH_3X + HX + 2X \rightleftharpoons CH_3CHCH_2X + 2HX + X$$

$$CH_3CHCH_2X + 2HX + X \rightleftharpoons CH_3CHCH_2 + 2HX + 2X$$

$$CH_3CHCH_2 + 2HX + 2X \rightleftharpoons H_2 + C_3H_6 + 4X$$

Scheme 2. The initial propane activated via the use of beta-carbon (that is, middle or second carbon) (**S2**).
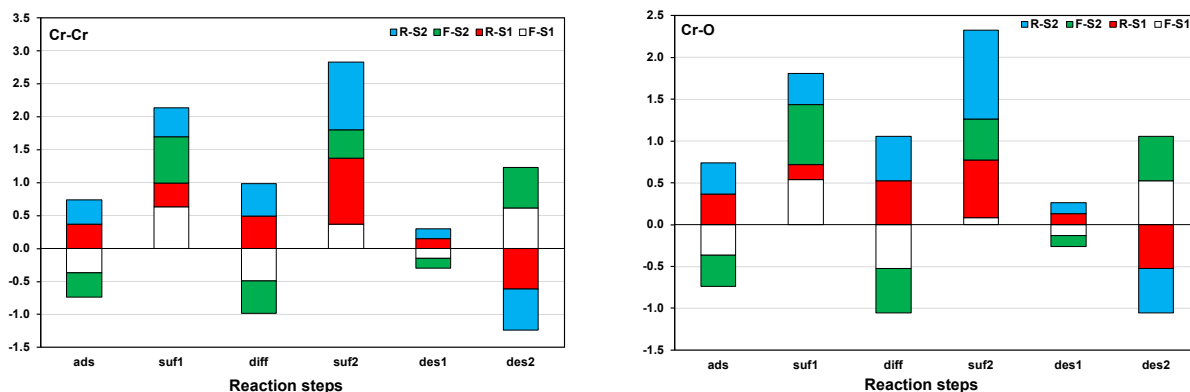
Figure 3. Energy barrier (E_a) in eV for the surface reaction steps across (a) Cr-Cr and (b) Cr-O paths, where 'ads,' 'des1', 'diff,' and 'suf1' stand for adsorption, desorption (similar to 'des2'), hydrogen diffusion, and surface reaction (similar for 'suf2'), respectively.

shows a good agreement with the experimental values similar to Nguyen *et al.* [22] report.

3.2. Energy barriers in reaction paths and the active sites in the elementary steps

The result collected for this study is diagrammatically represented in Figures 3 and 4. The figures display results for the Cr-Cr, Cr-O, O-Cr, and O-O sites. They indicate the different energy barriers collected for the different reaction steps in the dehydrogenation of propane. The R-S1 depicts the 'reverse reaction' in a form presented in Scheme 1 (that is, F represents the forward reaction, and R is the reverse). The six elementary reaction steps involved in the study are adsorption, first abstraction, diffusion, other abstraction, propylene desorption, and hydrogen desorption, and they are represented by 'ads,' 'suf1', 'diff,' 'suf2', 'des1' and 'des2', respectively.

Figure 3 shows that all forward reactions involved in the propane adsorption, hydrogen diffusion, and propylene desorption steps indicate the negative energy barrier(s). From the literature [33,34], these findings imply that they are barrierless steps, unlike the other steps, such as the hydrogen

abstraction and hydrogen desorption steps, which show positive activation energy (or energy barrier). These findings are similar to the results presented for O-Cr and O-O sites, as shown in Figure 4.

The evaluation of the elementary steps' energy barrier involved this reaction network indicates that the first abstraction of hydrogen shows a higher energy barrier. This step could have been responsible for retarding the reaction rate when the entire reaction process's energy is low. Moreover, the high energy barrier observed for the second hydrogen abstraction's reverse reaction indicates that it would be difficult for the step to be reversed due to the high energy barrier required to have the step reversed. The findings in Figures 3 and 4 were found to be the same for the evaluation carried out across the Cr-Cr, Cr-O, O-Cr, and O-O sites for the dehydrogenation of propane across the chromium oxide.

The energy barrier for the abstraction of the first hydrogen from the propane was in the trend: OO-S1 (0.86 eV) > OCr-S1 (0.86 eV) > CrCr-S1 (0.63 eV) > CrO-S1 (0.54 eV) and CrO-S2 (0.72 eV) > CrCr-S2 (0.70 eV) > OCr-S2 (0.70 eV) > OO-S2 (0.69 eV) in the reaction route of Scheme 1 and 2, respectively.
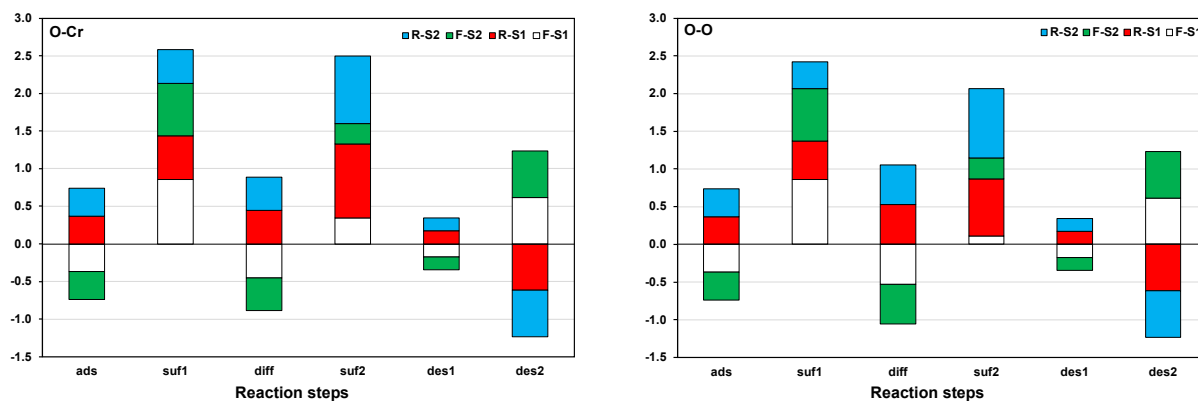
Figure 4. Energy barriers (E_a) in eV for the surface reaction steps across (a) O-Cr and (b) O-O paths, where 'ads,' 'des1', 'diff,' and 'suf1' stand for adsorption, desorption (similar to 'des2'), hydrogen diffusion, and surface reaction (similar for 'suf2'), respectively.
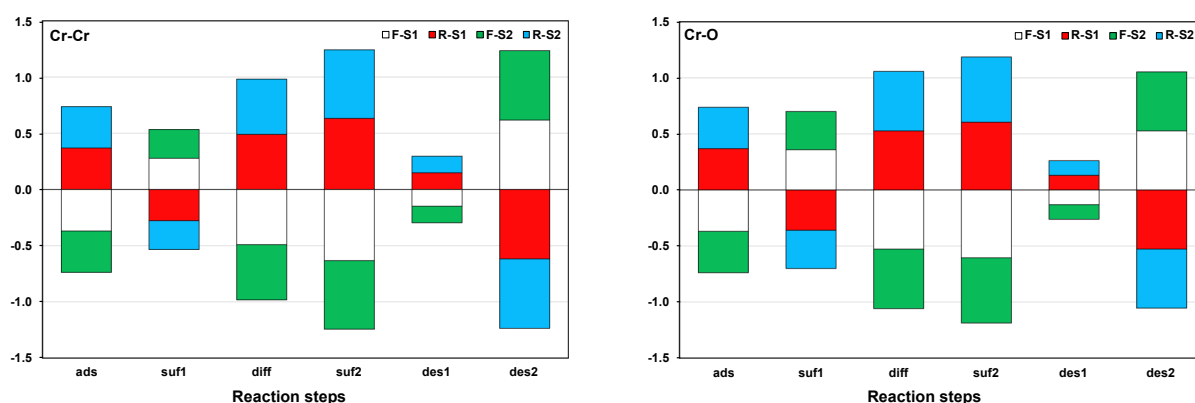
Figure 5. Reaction energy (ΔG) in eV for the reaction path across (a) Cr-Cr and (b) Cr-O sites, where 'ads,' 'des1', 'diff,' and 'suf1' stand for adsorption, desorption (similar to 'des2'), hydrogen diffusion, and surface reaction (similar for 'suf2'), respectively.
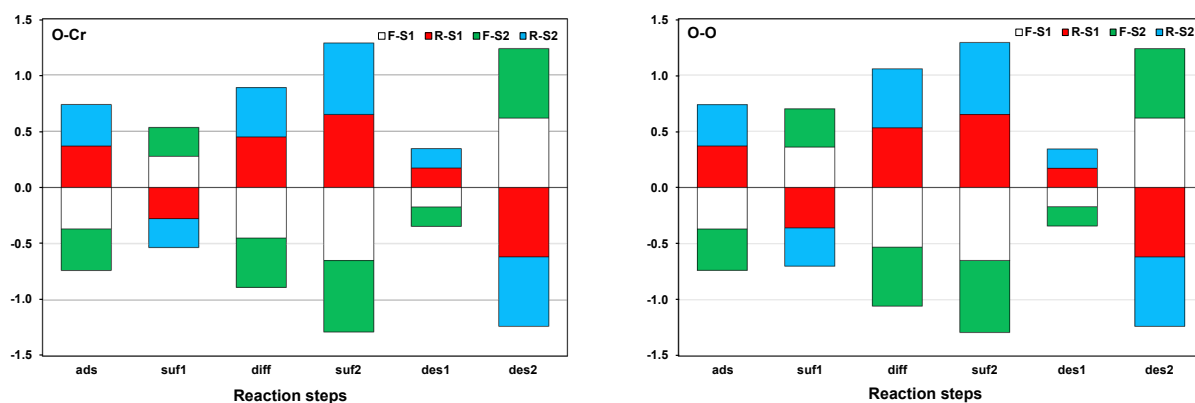
Figure 6. Reaction energy (ΔG) in eV for the reaction path across (a) O-Cr and (b) O-O sites, where 'ads,' 'des1', 'diff,' and 'suf1' stand for adsorption, desorption (similar to 'des2'), hydrogen diffusion, and surface reaction (similar for 'suf2'), respectively.

OO-S1 (0.86 eV) and OCr-S1 (0.86 eV) show the highest activation energy for the progression of the reaction at the first hydrogen abstraction step. In comparison, CrO-S1 (0.54 eV) was identified to have shown the least energy barrier.

The energy barrier for the abstraction of the second hydrogen from the adsorbed isopropyl was in the trend: CrCr-S1 (0.37 eV) > OCr-S1 (0.34 eV) > OO-S1 (0.11 eV) > CrO-S1 (0.09 eV) and CrO-S2 (0.48 eV) > CrCr-S2 (0.42 eV) > OO-S2 (0.28 eV) > OCr-S2 (0.26 eV) in the reaction route of Scheme 1 and 2, respectively. Similarly, CrO-S2 (0.48 eV) and CrCr-S2 (0.42 eV) show the highest energy barrier. In comparison, CrO-S1 (0.09 eV) was identified to have shown the least energy barrier for the reaction's progression at the second hydrogen

abstraction step. This finding implies that the Cr-O sites along the Scheme 1 route tend to reflect a lower energy barrier in its routes. This study shows that the active sites have a significant influence on the level of the energy barrier. It also shows that the propyl was adsorbed on the Cr site, while the H on the O site indicates that the Cr site remains an active component of the dehydrogenation reaction, as suggested in the literature [35]. These findings agree with the report of Yau *et al.* [5], which indicates that the metallic site plays a key role in getting propane dehydrogenated on the metallic oxide.

Similarly, the findings agreed with the report of Oyegoke *et al.* [10] on the chromium oxide sites' acidity reactivity, where Cr site was confirmed to be the most active site on a chromium oxide
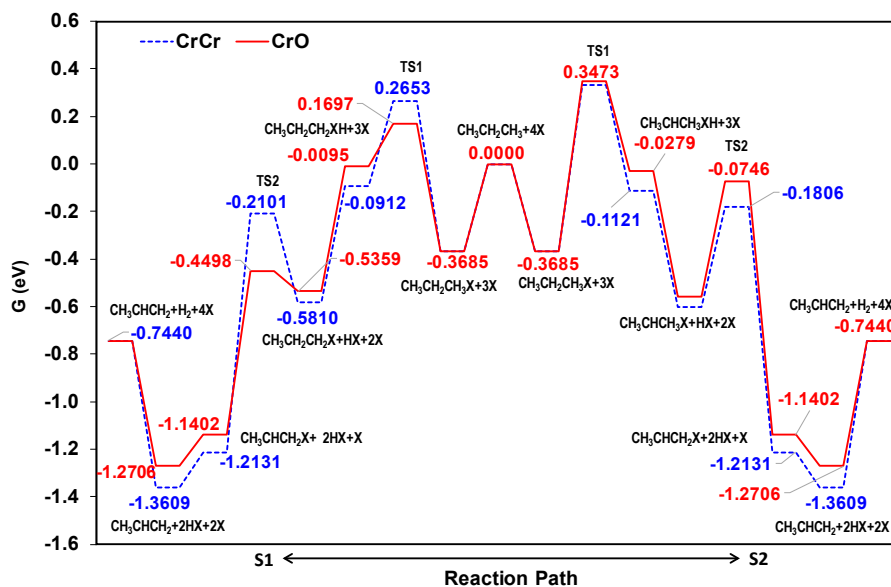
Figure 7. Propane dehydrogenation reaction path across Cr-Cr and Cr-O pair sites using the reaction Schemes 1 (LHS) and 2 (RHS) (All in eV), where LHS is the left-hand side, RHS is the right-hand side.
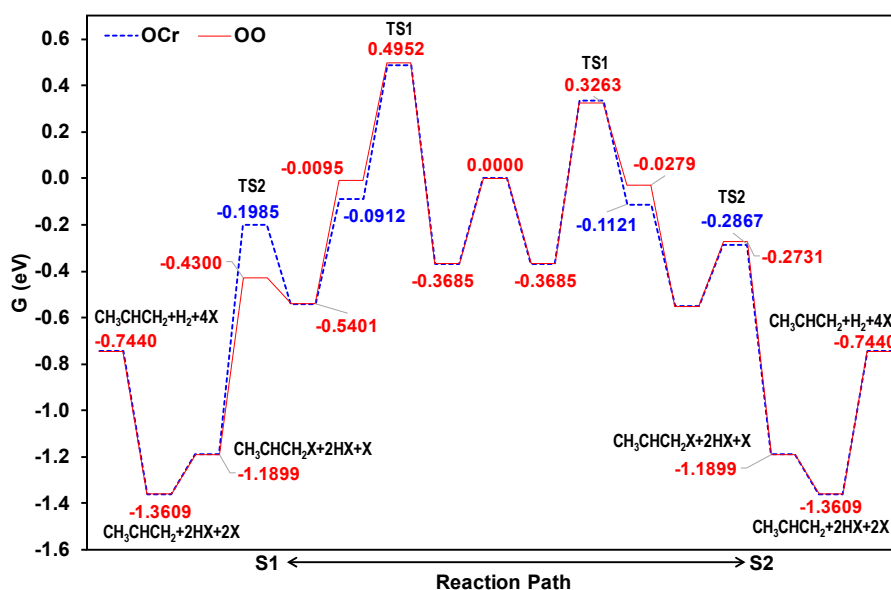

Figure 8. Propane dehydrogenation reaction path across O-Cr and O-O pair sites using the reaction Schemes 1 (LHS) and 2 (RHS) (All in eV).

catalyst. However, an excess concentration of these Cr sites would tend to promote the cracking of the propane into undesired products as reported in the literature [17] where the Cr-Cr reaction route was identified to be the path promoting cracking of propane into smaller molecules (methane, ethylene, and cokes) which could lead to coking of the catalyst.

3.3. Evaluation of the reaction energy demands and influence of the active sites

Figures 5 and 6 show the reaction energies for the forward reactions of the elementary steps in the propane dehydro-genation process. The figures indicate that all elementary steps have negative reaction energy, except for the first hydrogen abstraction and hydrogen desorption steps, which were positive. The findings imply that all elementary steps are exo-thermic steps except for the first hydrogen abstraction and hydrogen desorption steps, that are endothermic.

The reaction energy for the abstraction of the first hydrogen from propane was in the trend: OO-S1 (0.36 eV) > CrO-S1 (0.36 eV) > OCr-S1 (0.28 eV) > CrCr-S1 (0.28 eV) and OO-S2 (0.34 eV) > CrO-S2 (0.34 eV) > OCr-S2 (0.26 eV) > CrCr-S2 (0.26 eV) in the reaction route of Scheme 1 and 2, respectively. Thus, OO-S1 (0.36 eV) and CrO-S1 (0.36 eV) have the highest reaction energy for the progression of the reaction at the first hydrogen abstraction step, while OCr-S2 (0.26 eV) and CrCr-S2 (0.26 eV) has the least reaction energy. The findings reveal that all the reaction energies are positive, which indicates that the reaction step is endothermic, and more energy would be required to overcome this step.

The reaction energy shown in Figures 5 and 6 for the abstraction of the second hydrogen from the adsorbed isopropyl is in the trend: OO-S1 (-0.65 eV) < OCr-S1 (-0.65 eV) < CrCr-S1 (-0.63 eV) < CrO-S1 (-0.60 eV) and OO-S2 (-0.64 eV) < OCr-S2 (-0.64 eV) < CrCr-S2 (-0.61 eV) < CrOS2 (-0.58 eV) for reaction path of Scheme 1 and 2, respectively. This step of

abstracting the second hydrogen was found to have recorded negative reaction energy, which implies that the reaction step is exothermic, and the step would require less energy compared to the initial abstraction step.

Moreover, OO-S1 (-0.65 eV) and OCr-S1 (-0.65 eV) sites displayed the highest negative reaction energy. In comparison, CrO-S2 (-0.58 eV) was found to have shown the least negative reaction energy for the reaction's progression when abstracting the second hydrogen. From the overall assessment of the reaction energies required to get hydrogen desorbed, the Cr-O site was identified to have recorded the least reaction energy. This assessment indicates the influence of the active site on the level of the energy barrier.

3.4. Evaluation of thermodynamic feasibility of a different reaction route or path and the identification of potential rate-limiting steps in the dehydrogenation process

The energy profiles presenting the reaction pathways were used to identify the energetically feasible reaction path that leads to the production process across the chromium oxide surface while assessing the impact of different surface sites like Cr-Cr and Cr-O sites presented in Figure 7, while O-O and O-Cr sites in Figure 8, together with the identification of possible path for propane activation, i.e., alpha-C (i.e., Scheme 1) or beta-C (i.e., Scheme 2) on the catalyst.

The assessment of the six elementary steps involved in the dehydrogenation of propane across Cr-Cr, Cr-O, O-Cr, and O-O sites were evaluated. The assessment of the adsorption steps across all sites irrespective of schemes employed, Schemes 1 or 2 reveals that all reaction pathways were found to have shown a similar propane adsorption trend, indicating an exothermic process with a barrier less profile in the energy profile, as shown in both Figures 7 and 8.

Further studies of the results presented both in Figures 7 and 8, for the first abstraction or elimination of hydrogen atoms from the propane show that Scheme 1 (where the first abstraction was held across the alpha or terminal carbon of the propane, and the Cr-O site, i.e., Cr-O (Scheme 1) reaction path was found to have displayed the lowest energy barrier. While the reaction path involved the interaction of O-O site and the beta (middle) carbon atom site, i.e., O-O (Scheme 2), displayed the highest energy barrier indicating a higher energy demand for the reaction to hold along that reaction pathway. The deductions made from these profiles agree with that which was obtained from Figure 3, indicating that Cr-O (Scheme 1) reaction path has the lowest energy barrier for the 1st abstraction step. The first abstraction step across the reaction paths evaluated was all found to be endothermic. In addition, the reaction profiles on vanadium oxide presented in the report of Zhao *et al.* [36] indicate a similar trend with that shown in Figures 7 and 8 for the first abstraction step, which was found to have an endothermic barrier.

Moreover, the products (that is, adsorbed propyl) of the first abstraction step indicate that O-O (S1) and Cr-O (S1) record the least negative energy value while O-Cr (S2) and Cr-Cr (S2) show the most negative energy. The findings imply that O-Cr (S2) and Cr-Cr (S2) sites would yield more stable intermediate species on their site, while O-O (S1) and Cr-O (S1) would yield less stable species, as shown in Figures 7 and 8.

As the hydrogen gets diffused to another site on the catalyst, it was observed that the negativity of the species' energy increases for the different reaction pathways studied. This observation implies an increase in the stability of the species across the different reaction routes studied. Likewise, the second abstraction step for the removal of hydrogen from the isopropyl(s) was studied to identify the trend of the energy barrier obtainable across different reaction route as shown in Figures 7 and 8, where it was identified that the Cr-O (S2) (Figure 7) reaction route displayed the highest energy barrier.

At the same time, the O-O (S1) (Figure 8) and Cr-O (S1) (Figure 7) were found to record the least energy barriers for the step.

In the study of the desorption step in the energy profile, it was observed that the adsorbed propylene and hydrogen exhibit more negative energy across Cr-Cr (-1.21 eV) compared to Cr-O (-1.14 eV) sites in Figure 7. In the case of the O-Cr (-1.19 eV) and O-O (-1.19 eV) sites in Figure 7, the desorption steps were found to have a little less negative energy when compared to the Cr-Cr sites (which was found to be more negative). These findings indicate that the propylene and hydrogen would be more stable on Cr-Cr than other sites. Moreover, it can be said that there would exist a strong binding force on the Cr-Cr site, while Cr-O showed the weakest binding force. The weaker binding force would make hydrogen and propylene desorption across the Cr-O sites less energy-demanding than the Cr-Cr site. This deduction further indicates that the more the catalyst surface gets more concentrated/ largely dominated by the Cr site, the more difficult it would be to have propylene desorbed from the catalyst surface; instead, it would promote deep dehydrogenation to produce undesired products like propyne. This study, therefore, suggests the substitution of Cr site with possibly new metals or the intro-duction of oxidants as a way of aiding to prevent deep dehydrogenation (or propylene dehydrogenation) in the conversion of propane to propylene, which was similar to Sattler *et al.* [37] suggestion of adjusting catalyst composition or operating conditions.

Additionally, Chaowei *et al.* [38] suggest the option of introducing vacancy sites on the catalyst. The activity of Cr sites in dehydrogenation to be highly significant vigorously promoting hydrogen abstraction. However, if the Cr activity is not moderated, it can promote undesired products through deep dehydrogenation process. The deduction agrees with the report of Adam *et al.* [39], which indicated that the catalyst activity decreases with a rise in total Cr content of the catalyst and that Cr site is a crucial one which calls for depopulation of Cr site as a possible way of moderating its activity.

Moreover, the findings from the collective study of the reaction barriers involved in the different reaction routes unveil that the dehydrogenation of propane into propylene across the path of O-O and O-Cr sites would be less feasible from the thermodynamics point of view, due to the higher barriers present along its reaction path. Unlike the other paths like Cr-Cr and Cr-O sites, which displayed much lower energy barriers along their path, making the path more feasible energetically in general. This Cr-Cr (S1) path is well known for promoting deep dehydrogenation and higher product desorption, which would later result in undesired products, while the Cr-O (S1) was found to be primarily promoted by the production of propylene and lower product desorption barrier. Likewise, the characteristics deduced from this study for the Cr-Cr (S1) path identify it as a path that promotes deep dehydrogenation through its stronger affinity for surface species, which provide insight into why a fast deposit of coke on the catalyst surface and methane is promoted on this surface as reported by Sattler *et al.* [37] in their study.

However, the most thermodynamically possible reaction pathway for the dehydrogenation of propane into propylene on chromium oxide was found to be Cr-O (S1) due to its lower relative energy demand for its reaction pathway barriers compared to other paths. And the first abstraction step, where the first C-H bond activation of propane at the alpha (or terminal) carbon takes place on Cr site, and the abstracted H gets adsorbed on O site on that reaction path, was found to be the potential rate-determining step (RDS) due to its large activation complex which was relatively higher when compared to other barriers present along that reaction path as displayed in the profile for Cr-O (S1) in Figure 7. This finding was found to be similar to that reported by Yu-Jue *et al.* [40], and Zhao *et al.* [36], which also confirms the first C-H activation step (i.e.,

the first abstraction step) as its RDS for propane dehydrogenated on a metallic oxide (i.e., vanadium oxide).

The rate-determining step (RDS) obtained in this study was found to be similar to that which was identified by Oyegoke *et al.* [17], for the cracking of propane into small molecules, although the reaction path is different (Cr-O is feasible for propane dehydrogenation while Cr-Cr route is feasible for propane cracking). The energy barrier obtained for the second C-H abstraction step in this study was found to be lower than that barrier obtained by Oyegoke *et al.* [17] for the cracking of propyl specie on the path of Cr-Cr reaction route, which often leads to cracking of the molecule due to the high activity of the Cr sites present on the catalyst surface in agreement with literature [10]. Therefore, this suggests reducing Cr site dominance on the catalyst surface via the substitution of selected Cr sites or oxidant/oxygen use.

4. Conclusions

The potential reaction routes for propylene production from propane across the chromium (III) oxide surface were investigated, and insight into the kinetic and thermodynamics involved in the dehydrogenation process's reaction mechanism was gained via a density functional theory calculation and the use of a cluster approach. This investigation presents detailed insights on factors contributing to the unpleasant selectivity and rapid deactivation of chromium oxide catalyst despite its high activity as a way of providing preliminary information on its kinetics this from a theoretical point of view (at molecular scale) along with some suggestions on how the catalyst can be improved.

The results obtained from the study of the process reveal that out of the six elementary reaction steps involved in the reaction, two steps: the first hydrogen abstraction and hydrogen desorption, were identified as being endothermic. In contrast, other steps, including propane adsorption, hydrogen diffusion, and the second stage of hydrogen abstraction, were identified as being exothermic. The study of the energy profiles displaying the different reaction pathways studied, confirms Cr-O (S1) reaction pathway as the thermodynamically viable pathway that would promote propylene production. The reaction pathway activates the propane across the Cr-O site at the alpha (or terminal) carbon of the propane, where the propyl gets adsorbed to the Cr site, and H species get adsorbed to the O site. This study was also able to identify the first hydrogen abstraction step as the potential rate-determining step (RDS) for defining the rate of the propane dehydrogenation process. The RDS energy barrier was found to be 0.72 eV, and the step is endothermic with a reaction energy of 0.36 eV.

It was also shown that the significant participation of Cr sites in the propane dehydrogenation process would hinder propylene's desorption and promote undesired products due to the stronger affinity between the propylene and Cr-Cr site, which makes it more stable on the surface. As a result, the finding from this study recommends partial substitution of Cr site with relevant metals or the introduction of oxidants that may modify the Cr electronic structure and hence its overall activity as a way of decreasing the deep dehydrogenation (or propylene dehydrogenation) in the conversion of propane to propylene.

Acknowledgment

Disclosure statement DS

ORCID

Toyese Oyegoke
iD http://orcid.org/0000-0002-2026-6864
Fadimatu Nyako Dabai
iD http://orcid.org/0000-0001-8708-4726
Adamu Uzairu
iD http://orcid.org/0000-0002-6973-6361
Baba El-Yakubu Jibril
iD http://orcid.org/0000-0002-0323-2726

References

[1]. Wittcoff, H. A.; Reuben, B. G.; Plotkin, J. S. Ind. Organic Chemicals, 2nd Edition, Wittcoff: Wiley Online Library, 2000.
[2]. Philip, J. C. Survey of Industrial Chemistry, Springer, US, 2001.
[3]. Budavari, S. Propylene - The Merck Index, Twelfth Edition ed., New Jersey: Merck & Co., 1996.
[4]. Ren, Y.; Zhang, F.; Hua, W.; Yue, Y.; Gao, Z. *Catalysis Today* **2009**, *148(3-4)*, 316-322.
[5]. Yan, L.; Li, Z. H.; Lu, J; Fan, K. N. *J. Phys. Chem. C* **2008**, *112(51)*, 20382-20392.
[6]. Ming-Lei, Y.; Zhu, Y. A.; Zhou, X. G.; Sui, Z. J.; Chen, D. *ACS Catalysis* **2012**, *2*, 1247-1258.
[7]. Lauri, N.; Karoliina, H. *ACS Catalysis* **2013**, *3*, 3026-3030.
[8]. Timothy, H. Computational study of the catalytic dehydrogenation of propane on Pt and Pt3Ga catalyst, Published Thesis, Universiteit Gent, 2015, 168-169.
[9]. Stephanie, S.; Sabbe, M. K.; Galvita, V. V.; Redekop, E. A.; Reyniers, M. F.; Marin, G. B. *ACS Catalysis.* **2017**, *7(11)*, 7495-7508.
[10]. Oyegoke, T.; Dabai, F. N.; Uzairu, A.; Jibril, B. Y. *Bayero J. Pure App. Sci.* **2018**, *11(1)*, 178-184.
[11]. Zhang, J.; Zhou, R. J.; Chang, Q. Y.; Sui, Z. J.; Zhou, X.-G.; Chen, D.; Zhu, Y. A. *Catalysis Today* **2020**, in press, https://doi.org/10.1016/j.cattod.2020.02.023.
[12]. Araujo-Lopez, E.; Joos, L.; Vandegehuchte, B. D.; Sharapa, D. I.; Studt, F. *J. Phys. Chem. C* **2020**, *124(5)*, 3171-3176.
[13]. Ningning, K.; Xing, F.; Fangfang, L.; Lu, W.; Haiping, L.; Youyong, L.; Shuit-Tong, L. *ACS Nano* **2020**, *14(5)*, 5772-5779.
[14]. Keith, S.; Ka, W. C.; Jorge, A. M. B.; Dmitry, Z.; Olga, S.; Christophe, C. *J. Am. Chem. Soc.* **2018**, *140(37)*, 11674-11679.
[15]. Xie, Y.; Luo, R.; Sun, G.; Chen, S.; Zhao, Z. J.; Mu, R. *RSC Chem. Sci.* **2020**, *11*, 3845-3851.
[16]. Warren, J. H. A guide to molecular mechanics & quantum chemical calculations, Vol. 2, Irvine, CA: Wavefunction., 2003.
[17]. Oyegoke, T.; Dabai, F. N.; Uzairu, A.; Jibril, B. Y. *J. Serbian Chem. Soc.* **2020**, *85(10)*, 1-14, https://doi.org/10.2298/JSC200521044O.
[18]. Brown, P.; Forsyth, J.; Lelievre-Berna E.; Tasset, F. *J. Phys. Condens. Matter.* **2002**, *14*, 1957-1966.
[19]. Wang, Y.; Gong, X.; Wang, J. *Phys. Chem. Chem. Phys.* **2010**, *12(10)*, 2471-2477.
[20]. Compere, C.; Costa, D.; Jolly, L.; Mauger, E.; Giessner–Prettre, C. *New J. Chem.* **2000**, *24(12)*, 993-998.
[21]. Veliah, S.; Xiang, K.; Pandey, R.; Recio J.; Newsam, J. *J. Phys. Chem. B* **1997**, *102*, 1126-1135.
[22]. Nguyen, N. H.; Ngo, D. H.; Le, M. C. *J. Mol. Model* **2013**, *19*, 3233-3243.
[23]. Arjunan, V.; Rani, T.; Mythili, C.; Mohan, S. *Eur. J. Chem.* **2011**, *2(1)*, 70-76.
[24]. Panicker, C.; Varghese, H.; George, A.; Thomas, P. *Eur. J. Chem.* **2010**, *1(3)*, 173-178.
[25]. Laurendeau, N. M. Statistical Thermo.: Fundamentals & Applications, Cambridge, Cambridge Univ. Press, 2005.
[26]. Kennedy, I.; Geering, H.; Rose, M.; Crossan, A. *Entropy* **2019**, *21(5)*, 454, 1-24.
[27]. Hill, T. L. An Introduction to Statistical Thermodynamics, New York: Dover Publications Inc., 1960.
[28]. Campbell, C. T.; Sprowl, L. H.; Arnadottir, L. *J. Phys. Chem. C* **2016**, *120(19)*, 10283-10297.
[29]. Savara, A. *J. Phys. Chem. C* **2013**, *117(30)*, 15710-15715.

[30]. Sprowl, L. H.; Campbell, C. T.; Arnadottir, L. *J. Phys. Chem. C* **2017**, *121(17)*, 9655-9655.

[31]. Sprowl, L. H.; Campbell, C. T.; Arnadottir L. *J. Phys. Chem. C* **2016**, *120(18)*, 9719-9731.

[32]. Bio-Rad, SpectraBase BIO-RAD, John Wiley & Son Inc., Wiley SpectraBase; SpectraBase Compound ID=4AmhtLT3JGD SpectraBase Spectrum ID=K4fPRHBxDI3 http://spectrabase.com/spectrum/K4fPRHBxDI3 (accessed Sep 29, 2020).

[33]. Peter, A.; Paula, J. D.; Keeler, J. Physical Chemistry, Oxford, Oxford University Press, 2018.

[34]. Houston, P. L. Chemical Kinetics & Reaction Dynamics, New York, Dover Publisher Inc, 2001.

[35]. Jibril, B. Y. *Appl. Cat. A: Gen.* **2004**, *264*, 193-202.

[36]. Zhao, Z. J.; Wu, T.; Xiong, C.; Sun, G.; Mu, R.; Zeng, L.; Gong, J. *Angw. Chem. Intl. Ed.* **2018**, *57(23)*, 6791-6795.

[37]. Sattler, J. J. H. B.; Ruiz-Martinez, J.; Santillan-Jimenez, E.; Weckhuysen, B. M. *Chem. Rev.* **2014**, *114(20)*, 10613-10653.

[38]. Si, C.; Lian, Z.; Olanrele, S. O.; Sun, X.; Li, B. *Appl. Surf. Sci.* **2020**, *519*, 146241.

[39]. Adam, W.; Jarczewski, S.; Wegrzynowicz, A.; Michorczyk, B.; Michorczyk, P. *Nanomaterials* **2017**, *7(249)*, 7-8.

[40]. Yu-Jue, D.; Li, Z. H.; Fan, K. N. *J. Mol. Catal. A: Gen.* **2013**, *379*, 122-138.